Supporting Information

Raghuraman et al. 10.1073/pnas.1314875111

SI Materials and Methods

Cloning, Mutagenesis, and Channel Biochemistry. We used pQE32 vector encoding the KcsA gene with a cysteine mutation at desired positions and for protein expression, as described by Cortes and Perozo (1). Mutations were carried out using QuikChange (Stratagene) site-directed mutagenesis. For EPR measurements, purified mutants were spin-labeled with methane thiosulfonate spin label (Toronto Research) and reconstituted in palmitoyloleoylphosphatidyl choline/palmitoyloleoylphosphatidyl glycerol (POPC/POPG) (3:1) liposomes as described previously (2). Distance measurements [both continuous wave (CW) EPR and pulsed EPR] were done using tandem dimer (TD) constructs of KcsA. TD constructs of cysteine mutants corresponding to outer vestibule residues of KcsA (positions 52–54, 56–58, 60, 81, 82, and 84–86) were constructed by cloning the cysteine mutant containing KcsA in the B protomer of the TD construct. The TD constructs were expressed and purified as described previously (2), resulting in a KcsA tetramer in which only the diagonal subunits had the desired mutation(s). Channels with cysteine mutants corresponding to positions 51, 53, 55, and 59 were not included in any measurements due to purification issues in either WT type or E71A background. For CW-EPR distance measurements, we made full-label and under-label samples, and the spin labeling was done at 1:10 (monomer/label) and 10:1 (monomer/label) molar ratios in ice for 1 h to prepare the full-label and under-label samples, respectively.

For fluorescence measurements, the purified cysteine mutants of KcsA were selectively labeled with the environment-sensitive fluorophore NBD (7-nitrobenz-2-oxa-1,3-diazol-4-yl) using *N*,*N*′-dimethyl-*N*-(iodoacetyl)-*N*′-(7-nitrobenz-2-oxa-1,3-diazol-4-yl) ethylenediamine (Invitrogen) dissolved in DMSO at a 1:10 (monomer/label) molar ratio in ice for 1 h. The excess dye was removed using a PD10 column, and the subsequently labeled KcsA tetramer was separated using gel filtration. The labeled mutants (~250 μg) were reconstituted in POPC/POPG (3:1) liposomes at a 1:1,000 (protein/lipid) molar ratio with added biobeads to remove the detergent. After high-speed ultracentrifugation, the proteoliposomes were resuspended in 20 mM Tris, 200 mM KCl (pH 7.5) buffer (closed state) and citrate phosphate (pH 4) buffer (open state).

Fluorescence Spectroscopy. Steady-state fluorescence measurements were performed with a Photon Technology Instruments spectrofluorometer using 1-cm pathlength quartz cuvettes. For the fluorescence emission scans and red edge excitation shift (REES) measurements, excitation and emission slits with a bandpass of 1 nm were used for all measurements. Background intensities of samples were subtracted from each sample spectrum to cancel out any contribution due to the solvent Raman peak and other scattering artifacts. The spectral shifts obtained with different sets of samples were identical in most cases. In other cases, the values were within ± 0.5 nm of those reported.

The wavelength-selective fluorescence approach in general and REES in particular represent a unique and powerful approach that can be used to monitor the environment-induced restriction and dynamics around a fluorophore in a complex biological system directly (reviewed in refs. 3–8). REES is operationally defined as the shift in the wavelength of maximum fluorescence emission toward higher wavelengths, caused by a shift in the excitation wavelength toward the red edge of the absorption band. The genesis of REES lies in the change in fluorophore–solvent interactions in the ground and excited states brought about by a change in the dipole moment of the fluorophore upon excitation, and the rate at which solvent molecules reorient around the excited-state fluorophore. In other words, this phenomenon arises from slow rates of solvent relaxation (reorientation) around an excited-state fluorophore and depends on the motional restriction in the immediate vicinity of the fluorophore. Through this approach, it is possible to evaluate the local dynamics of the environment itself (which are represented by the relaxing solvent molecules) using a fluorophore merely as a reporter group.

For a polar fluorophore (like NBD) in a bulk nonviscous solvent, the reorientation of solvent (water in biological systems) molecules occurs at a time scale of the order of picoseconds, so that all the solvent molecules completely reorient around the excited state dipole of the fluorophore well within its excited lifetime, which is typically of the order of nanoseconds. Hence, irrespective of the excitation wavelength used (465–515 nm in our case), emission is observed only from the solvent-relaxed state and no REES will be observed (i.e., 0-nm REES). However, if the same fluorophore is placed in a motionally restricted environment (e.g., viscous medium, membranes, membrane proteins), the process of reorientation of solvent molecules is slowed down to nanoseconds or longer. Hence, changing the excitation wavelength toward the red edge of the absorption band (465–515 nm) selectively excites those fluorophores that interact more strongly with the solvent molecules in the excited state. These are the fluorophores around which the solvent molecules are oriented in such a way as to be more similar to those found in the solvent-relaxed state. Thus, the necessary condition for giving rise to REES is that a different average population of fluorophores is excited at each excitation wavelength, which requires the dipolar relaxation time for the solvent shell to be comparable to or longer than the fluorescence lifetime, so that fluorescence occurs from various partially relaxed states. This gives rise to different magnitudes of REES and implies reduced mobility of the surrounding matrix with respect to the fluorophore. The REES approach has been widely used to monitor the organization and dynamics of membranes and membrane/mimetic systems (9–13), lipid–protein interactions (14–17), and folding and topology of soluble and membrane proteins (17–19).

Fluorescence polarization measurements were performed at room temperature (~23 °C), and the polarization values were calculated as described previously (20). All experiments were done with three sets of samples, and the polarization values shown in Fig. 2 and Fig. S2 represent mean ± SE.

Liposome Patch-Clamp. Electrophysiological measurements of proteoliposomes were made using the patch-clamp as described earlier (21). Macroscopic currents were measured at a 1:1,000 (moles/moles) ratio under symmetrical conditions in 5 mM 3(N-morpholino) propanesulfonic acid (Mops), 200 mM KCl (pH 4.0) buffer after a pH jump using an RCS-160 fast-solution exchanger (Biologic). Pipette resistances were ~2 MΩ.

EPR Spectroscopy and Distance Measurements. CW-EPR spectra at room temperature were obtained for spin-labeled, reconstituted channels as described for closed (pH 7) and open (pH 4) channels, using a Bruker EMX spectrometer equipped with a loop-gap resonator under the following conditions: 2-mW incident power, 100-kHz modulation frequency, 1-G modulation amplitude, 41-ms conversion time, and 41-ms time constant. Changes in pH were made by resuspending the KcsA-containing liposomes in Tris·KCl buffer (pH 7) and citrate phosphate buffer (pH 4).

CW-EPR distance measurements in the closed and open states were made in POPC/POPG (3:1) proteoliposomes at 130 K in presence of liquid N_2 using <50 μW of incident power to avoid saturation of the signal. Full-label and under-label spectra were measured under identical conditions, and the distances were estimated using the dipolarly broadened CW spectra analysis program CWdipol (22).

Double Electron-Electron Resonance Spectroscopy. Double electron-electron resonance (DEER) spectroscopy is a powerful pulse EPR approach that allows the determination of spin-spin distance and distance distributions between spin labels on soluble and membrane proteins in their native environment (reviewed in refs. 23–26, also see refs. 27–29). This pulsed EPR approach extracts weaker dipolar interactions from spin coherence, and is therefore sensitive to measuring longer interspin distances (~20–60 Å). The DEER signal is a modulation of the echo amplitude of one spin population when another spin population is excited with intense microwave radiation while changing the timing of the excitation. DEER measurements were carried out using a Bruker ELEXYS E580 X-band pulsed spectrometer operating near 9.7 GHz and equipped with a split-ring MS2 resonator at a temperature of 55 K using liquid helium. This temperature was used to achieve the highest signal-to-noise ratio as T1 (spin-lattice) and T2 (spin-spin) relaxations gained optimal values (26). Spin-labeled TD constructs of KcsA reconstituted in POPC/POPG (3:1) liposomes were used. The pelleted proteoliposomes were then transferred to quartz 1.1 × 1.6 × 100-mm capillaries and flash-frozen to 55 K in the resonator. All the measurements were performed using a constant-time version of the four-pulse DEER sequence $\pi/2(\nu_{obs}) - \tau_1 - \pi(\nu_{obs}) - t' - \pi(\nu_{pump}) - (\tau_1 + \tau_2 - t') - \pi(\nu_{obs}) - \tau_2 -$ echo (30), where time t' is varied, using the pulseSPEL program (Bruker). The resonator was overcoupled to $Q \sim$ 100–200, the pump frequency (ν_{pump}) was set to the center of the resonator dip and coincided with the maximum of the nitroxide EPR spectrum, and the observer frequency (ν_{obs}) was set 65–70 MHz higher and coincided with the low-field local maximum of the spectrum. The pulse lengths for $\pi/2$ and π were 16 ns and 32 ns, respectively, and the pump pulse length was 28–36 ns. The pump pulse and inversion pump lengths were optimized using a nutation experiment for all cases. In all experiments, a τ_1 of 200 ns was used. Data were recorded typically at steps of 12 ns. Accumulation times for the different datasets varied between 8 and 16 h. Data were processed and analyzed using the program DEER Analysis 2008 (31). A homogeneous 3D background model was used to subtract intermolecular background from raw data. The criterion for choosing background subtraction was the frequency-domain spectrum, where neither a positive spike nor an obvious hole was present in the center of the Pake pattern. Computation of an L-curve was performed to choose the optimal value for the Tikhonov regularization parameter, which corresponded to the corner of the L-curve.

Restrained Ensemble Simulations. A recently developed molecular dynamics simulation technique, the restrained ensemble (RE) method (32, 33), was used to refine the outer vestibule structure of KcsA in various functional states. The crystal structures of KcsA corresponding to closed/conductive [Protein Data Bank (PDB) ID code 1K4C] (34), open/inactivated (PDB ID code 3F5W) (35), and "flipped" E71A (PDB ID code 2ATK) (21) were used to construct the initial geometry for the RE simulations. The simulations were carried out with the CHARMM (36) program suite, using the all-atom CHARMM27 protein force field (37) with the CMAP corrections (38) and the nitroxide spin-label force field parameters (39). For each of the crystal structures, six structures were made, with each containing only two spin labels at positions 52–56, 53–82, 54–81, 57–86, 58–85, and 60–84, thus avoiding steric clashes. Each KcsA tetramer therefore contained a total of eight spin labels giving a total of four distances. Due to the tetrameric arrangement, data on a total of 24 diagonal spin-pair distance distributions were used for the six RE simulations. Except for the selectivity filter and the surrounding support structures (residues 51–65 and 75–88), the rest of the system is fixed to its X-ray crystallographic structure, and the outer vestibule was completely solvated by TIP3P water molecules. A weak harmonic restraint with a force constant of 1 kcal·mol·Å^2 was applied to the backbone of the outer vestibule to avoid any large motion. Before RE simulation, spin labels at a particular site were replicated 25 times, giving a total of 625 distances (25 * 25) between ensembles of diagonal spin-label pairs, which provides the calculated distance distributions. A force constant of 100,000 kcal/mol was used to impose the energy restraint to match the calculated distributions with those of the experiment. The distance distributions obtained from simulation are very similar to those obtained from the experiments (Figs. S7 and S8). The RE simulations were performed as described (12, 13) for 1 ns, from which an average structure was obtained. Six average structures thus obtained from six different RE simulations were again averaged to obtain the final structure, and backbone rmsd deviation was calculated with respect to the X-ray crystal structure. Following the above procedure, the average structure obtained from the first cycle was again used to perform six different RE simulations; a new average structure is obtained and rmsd deviation is calculated. These cycles are continued until the rmsd deviation with respect to the X-ray crystal structure flattens out, and this process is continued for all four KcsA structures (Fig. 4*C*). The converged structures thus obtained are the refined structures of the KcsA in their various functional states, which are then used for further analysis.

1. Cortes DM, Perozo E (1997) Structural dynamics of the *Streptomyces lividans* K^+ channel (SKC1): Oligomeric stoichiometry and stability. *Biochemistry* 36(33): 10343–10352.
2. Liu Y-S, Sompornpisut P, Perozo E (2001) Structure of the KcsA channel intracellular gate in the open state. *Nat Struct Biol* 8(10):883–887.
3. Raghuraman H, Kelkar DA, Chattopadhyay A (2005) Novel insights into protein structure and dynamics utilizing the red edge excitation shift. *Reviews in Fluorescence 2005*, eds Geddes CD, Lakowicz JR (Springer, New York), pp 199–222.
4. Demchenko AP (2008) Site-selective Red-Edge effects. *Methods Enzymol* 450:59–78.
5. Chattopadhyay A, Haldar S (2013) Dynamic insight into protein structure utilizing red edge excitation shift. *Acc Chem Res*, 10.1021/ar400006z.
6. Raghuraman H, Kelkar DA, Chattopadhyay A (2003) Novel insights into membrane protein structure and dynamics utilizing the wavelength-selective fluorescence approach. *Proceedings of the Indian National Science Academy* 69(1):25–35.
7. Chattopadhyay A (2003) Exploring membrane organization and dynamics by the wavelength-selective fluorescence approach. *Chem Phys Lipids* 122(1-2):3–17.
8. Demchenko AP (2002) The red-edge effects: 30 years of exploration. *Luminescence* 17(1):19–42.
9. Mukherjee S, Raghuraman H, Dasgupta S, Chattopadhyay A (2004) Organization and dynamics of N-(7-nitrobenz-2-oxa-1,3-diazol-4-yl)-labeled lipids: A fluorescence approach. *Chem Phys Lipids* 127(1):91–101.
10. Raghuraman H, Pradhan SK, Chattopadhyay A (2004) Effect of urea on the organization and dynamics of Triton X-100 micelles: A fluorescence approach. *J Phys Chem B* 108(7):2489–2496.
11. Arora A, Raghuraman H, Chattopadhyay A (2004) Influence of cholesterol and ergosterol on membrane dynamics: A fluorescence approach. *Biochem Biophys Res Commun* 318(4):920–926.
12. Mukherjee S, Raghuraman H, Chattopadhyay A (2007) Membrane localization and dynamics of Nile Red: Effect of cholesterol. *Biochim Biophys Acta* 1768(1):59–66.
13. Raghuraman H, Shrivastava S, Chattopadhyay A (2007) Monitoring the looping up of acyl chain labeled NBD lipids in membranes as a function of membrane phase state. *Biochim Biophys Acta* 1768(5):1258–1267.
14. Raghuraman H, Chattopadhyay A (2004) Interaction of melittin with membrane cholesterol: A fluorescence approach. *Biophys J* 87(4):2419–2432.
15. Raghuraman H, Chattopadhyay A (2004) Influence of lipid chain unsaturation on membrane-bound melittin: A fluorescence approach. *Biochim Biophys Acta* 1665(1-2):29–39.

16. Haldar S, Raghuraman H, Namani T, Rajarathnam K, Chattopadhyay A (2010) Membrane interaction of the N-terminal domain of chemokine receptor CXCR1. *Biochim Biophys Acta* 1798(6):1056–1061.
17. Rawat SS, Kelkar DA, Chattopadhyay A (2004) Monitoring gramicidin conformations in membranes: A fluorescence approach. *Biophys J* 87(2):831–843.
18. Raghuraman H, Chattopadhyay A (2006) Effect of ionic strength on folding and aggregation of the hemolytic peptide melittin in solution. *Biopolymers* 83(2):111–121.
19. Tory MC, Merrill AR (2002) Determination of membrane protein topology by red-edge excitation shift analysis: Application to the membrane-bound colicin E1 channel peptide. *Biochim Biophys Acta* 1564(2):435–448.
20. Raghuraman H, Chattopadhyay A (2003) Organization and dynamics of melittin in environments of graded hydration. *Langmuir* 19(24):10332–10341.
21. Cordero-Morales JF, et al. (2006) Molecular determinants of gating at the potassium-channel selectivity filter. *Nat Struct Mol Biol* 13(4):311–318.
22. Sen KI, Logan TM, Fajer PG (2007) Protein dynamics and monomer-monomer interactions in AntR activation by electron paramagnetic resonance and double electron-electron resonance. *Biochemistry* 46(41):11639–11649.
23. Jeschke G (2012) DEER distance measurements on proteins. *Annu Rev Phys Chem* 63: 419–446.
24. Schiemann O, Prisner TF (2007) Long-range distance determinations in biomacromolecules by EPR spectroscopy. *Q Rev Biophys* 40(1):1–53.
25. McHaourab HS, Steed PR, Kazmier K (2011) Toward the fourth dimension of membrane protein structure: Insight into dynamics from spin-labeling EPR spectroscopy. *Structure* 19(11):1549–1561.
26. Fajer PJ, Brown L, Song L (2007) Practical pulsed dipolar ESR (DEER). *ESR Spectroscopy in Membrane Biophysics,* Biological Magnetic Resonance (Springer, New York), Vol 27, pp 95-128.
27. Torbeev VY, et al. (2009) Dynamics of "flap" structures in three HIV-1 protease/inhibitor complexes probed by total chemical synthesis and pulse-EPR spectroscopy. *J Am Chem Soc* 131(3):884–885.
28. Torbeev VY, et al. (2011) Protein conformational dynamics in the mechanism of HIV-1 protease catalysis. *Proc Natl Acad Sci USA* 108(52):20982–20987.
29. White EA, Raghuraman H, Perozo E, Glotzer M (2013) Binding of the CYK-4 subunit of the centralspindlin complex induces a large scale conformational change in the kinesin subunit. *J Biol Chem* 288(27):19785–19795.
30. Pannier M, Veit S, Godt A, Jeschke G, Spiess HW (2000) Dead-time free measurement of dipole-dipole interactions between electron spins. *J Magn Reson* 142(2):331–340.
31. Jeschke G, et al. (2006) DEER Analysis 2006—A comprehensive software package for analyzing pulsed ELDOR data. *Appl Magn Reson* 30(3-4):473–498.
32. Roux B, Islam SM (2013) Restrained-ensemble molecular dynamics simulations based on distance histograms from double electron-electron resonance spectroscopy. *J Phys Chem B* 117(17):4733–4739.
33. Islam SM, Stein RA, McHaourab HS, Roux B (2013) Structural refinement from restrained-ensemble simulations based on EPR/DEER data: Application to T4 lysozyme. *J Phys Chem B* 117(17):4740–4754.
34. Zhou Y, Morais-Cabral JH, Kaufman A, MacKinnon R (2001) Chemistry of ion coordination and hydration revealed by a K+ channel-Fab complex at 2.0 A resolution. *Nature* 414(6859):43–48.
35. Cuello LG, Jogini V, Cortes DM, Perozo E (2010) Structural mechanism of C-type inactivation in K(+) channels. *Nature* 466(7303):203–208.
36. Brooks BR, et al. (2009) CHARMM: The biomolecular simulation program. *J Comput Chem* 30(10):1545–1614.
37. MacKerell AD, et al. (1998) All-atom empirical potential for molecular modeling and dynamics studies of proteins. *J Phys Chem B* 102:3586–3616.
38. Mackerell AD, Jr., Feig M, Brooks CL, 3rd (2004) Extending the treatment of backbone energetics in protein force fields: Limitations of gas-phase quantum mechanics in reproducing protein conformational distributions in molecular dynamics simulations. *J Comput Chem* 25(11):1400–1415.
39. Sezer D, Freed JH, Roux B (2008) Parametrization, molecular dynamics simulation, and calculation of electron spin resonance spectra of a nitroxide spin label on a polyalanine α-helix. *J Phys Chem B* 112(18):5755–5767.

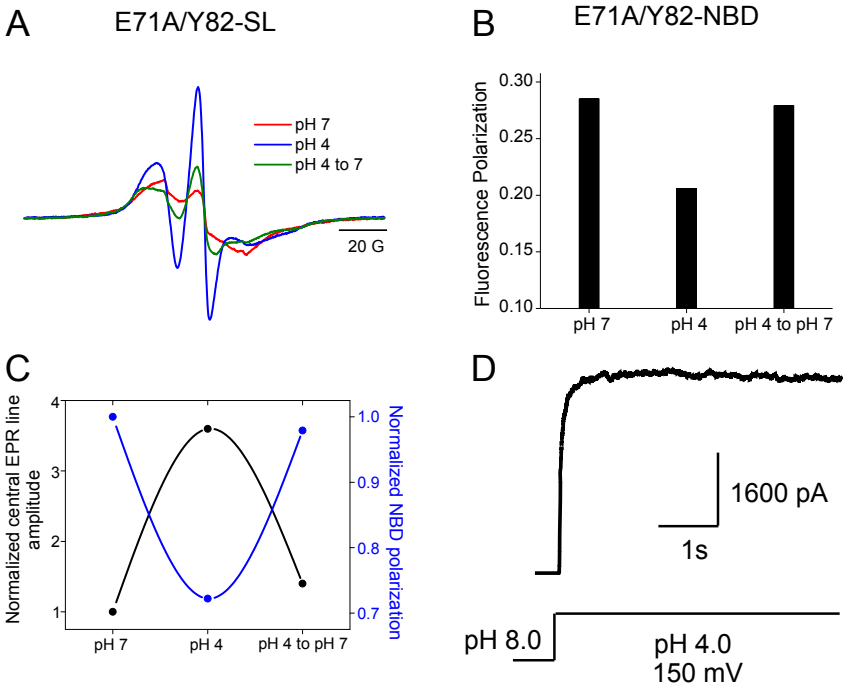

Fig. S1. Spin-labeled and NBD-labeled E71A/Y82C constructs are functional, and the conformational changes observed are reversible. CW-EPR spectra of E71A/Y82-SL KcsA (*A*) and steady-state polarization of NBD fluorescence measured for E71A/Y82-NBD KcsA (*B*) reconstituted in POPC/POPG (3:1, moles/moles) liposomes are shown. Measurements at pH 7.5 and pH 4 correspond to closed and open states of the channel. The excitation wavelength used was 480 nm; emission was monitored at 535 nm in all cases. The polarization values represent the mean of three independent measurements. The error is typically <2–5% of the reported values. (*C*) Reversibility of dynamics of E71A/Y82-SL and E71A/Y82-NBD KcsA. The lines drawn are merely visual aids. (*D*) Normalized macroscopic current of E71A/Y82-NBD KcsA was elicited by pH jumps from 8.0 to 4.0 using a rapid solution exchanger with a membrane potential held at +150 mV. Similar functional behavior was observed for E71A/Y82-SL KcsA. Details are provided in *SI Materials and Methods*.

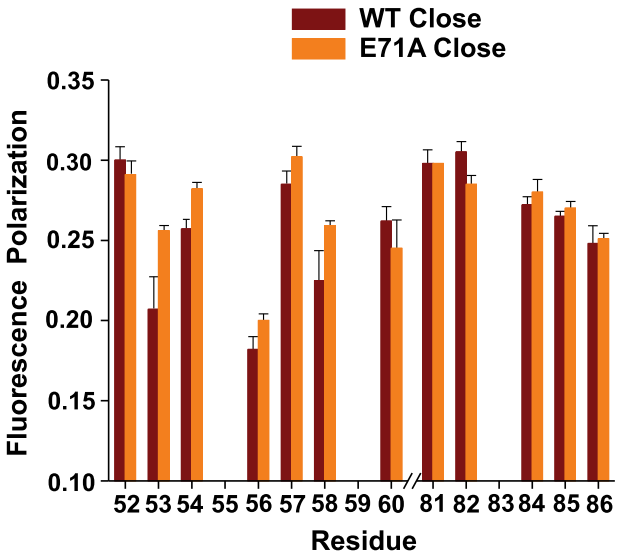

Fig. S2. Dynamics of the outer vestibule in closed states of WT and E71A KcsA are similar. A comparison of steady-state polarization of NBD fluorescence measured for NBD-labeled outer vestibule residues of full-length WT (brown) and E71A (orange) KcsA reconstituted in POPC/POPG (3:1, moles/moles) liposomes was made. Measurements were carried out at pH 7.5 to stabilize the closed states of the channel. The excitation wavelength used was 480 nm; emission was monitored at 535 nm in all cases. The polarization values represent mean ± SE of three independent measurements. Details are provided in *SI Materials and Methods*.

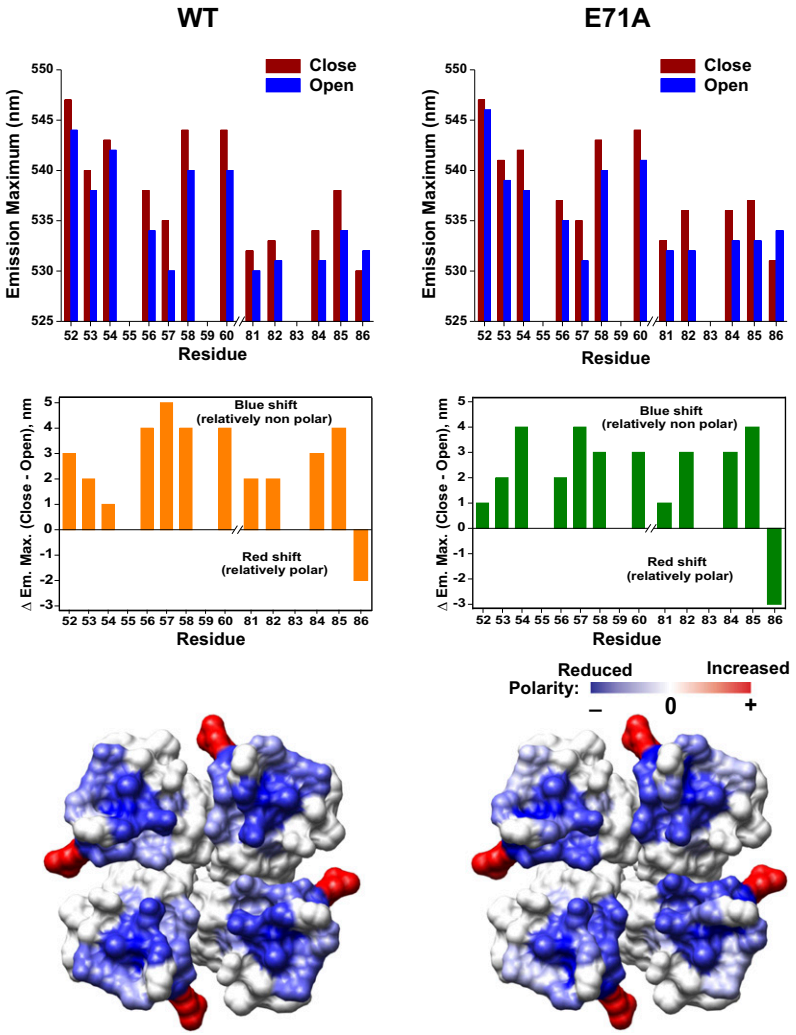

Fig. S3. Gating-related local polarity changes in inactivated and conductive states of KcsA are similar. Fluorescence emission maximum of NBD fluorescence measured for NBD-labeled outer vestibule residues of WT (*Left*) and E71A (*Right*) KcsA reconstituted in POPC/POPG (3:1, moles/moles) liposomes (*Top*). Measurements at pH 7.5 and pH 4 correspond to closed and open states of the channel. The excitation wavelength used was 480 nm in all cases. The difference in emission maximum values (ΔEm. Max.) are shown (*Middle*), and the difference values were mapped on the crystal structure of KcsA (1K4C) to highlight the changes in polarity of the microenvironment of the fluorophore between different functional states of KcsA upon gating (*Bottom*). Details are provided in *SI Materials and Methods*.

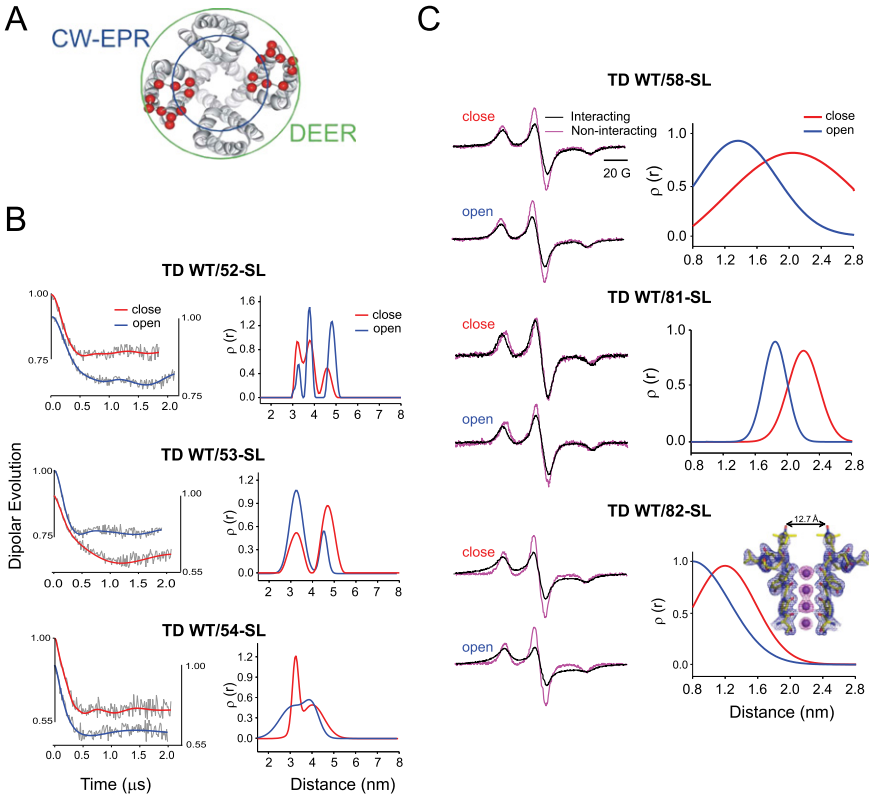

Fig. S4. Comparison of distance distributions corresponding to outer vestibule residues in closed and open states of WT KcsA in membranes. (*A*) Top view of TD KcsA showing the outer vestibule cysteine mutants (red spheres), between diagonally symmetrical subunits, used for distance measurements. (*B*) Long distances were probed by DEER at 55 K in the presence of liquid He. The dipolar evolution curves, along with the distance distributions for indicated TD constructs, are shown for closed (red) and open (blue) states of WT KcsA reconstituted in POPC/POPG (3:1, moles/ moles) liposomes. (*C*) Short distances were measured by CW-EPR between spin labels bound to diagonally placed cysteine residues in the indicated TD constructs. The measurements were made in proteoliposomes at 130 K in the presence of liquid N_2 using <50 mW of incident power to avoid saturation of the signal. The fully labeled (interacting) and underlabeled (noninteracting) EPR spectra for closed and open states (*Left*) and the distance distributions (*Right*) are shown. (*Inset*) Crystal structure of the spin-label–bound Y82C KcsA [PDB ID code 3STZ (24)] is shown, and the distance between the N and O groups of the spin label from diagonally symmetrical subunits is labeled (black arrow). Details are provided in *SI Materials and Methods*.

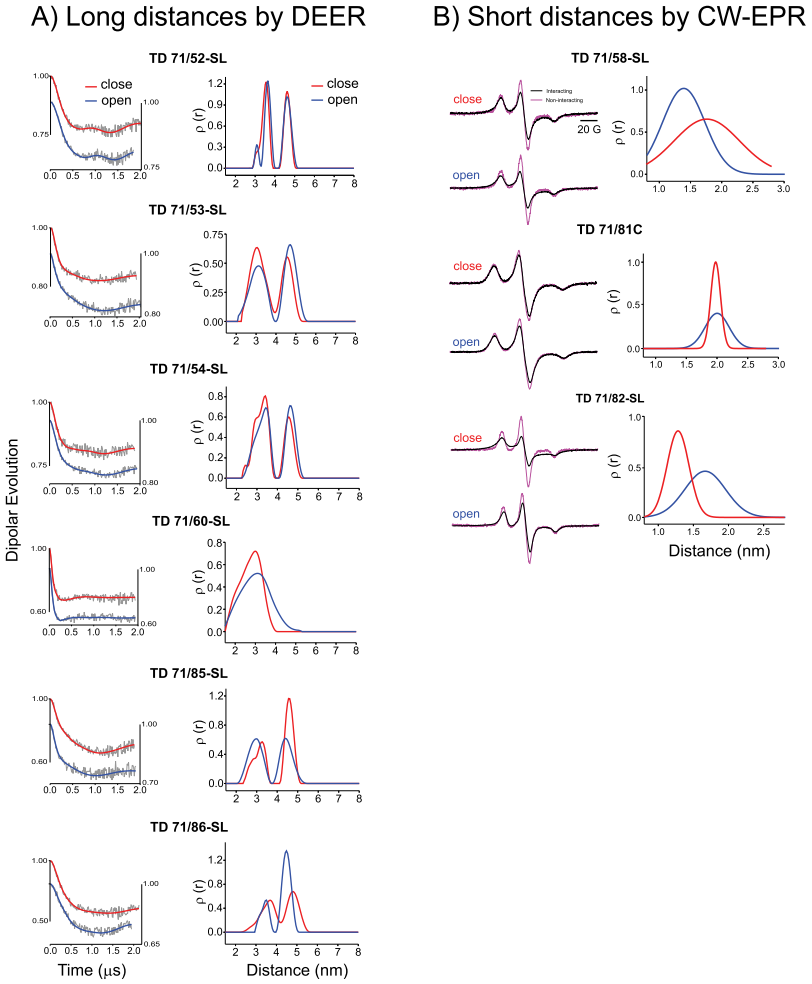

Fig. S5. Comparison of distance distributions corresponding to the outer vestibule residues in closed and open states of E71A KcsA in membranes. (*A*) Long distances were probed by DEER at 55 K in the presence of liquid He. The dipolar evolution curves, along with the distance distributions for indicated TD constructs, are shown for closed (red) and open (blue) states of WT KcsA reconstituted in POPC/POPG (3:1, moles/moles) liposomes. (*B*) Short distances were measured by CW-EPR between spin labels bound to diagonally placed cysteine residues in the indicated TD constructs. The measurements were made in proteoliposomes at 130 K in the presence of liquid N_2 using <50 mW of incident power to avoid saturation of the signal. The fully labeled (interacting) and underlabeled (noninteracting) EPR spectra for closed and open states (*Left*) and the distance distributions (*Right*) are shown. Details are provided in *SI Materials and Methods*.

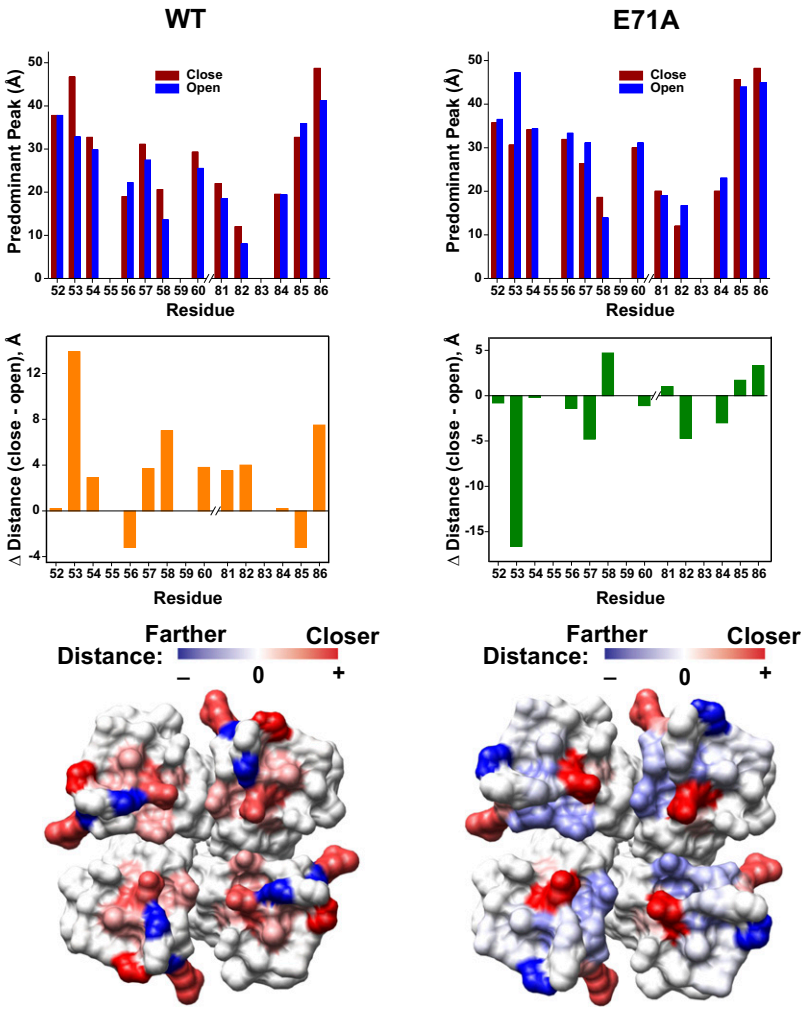

Fig. S6. Predominant peak distance analysis. Predominant distances of spin-labeled outer vestibule residues of WT (*Left*) and E71A (*Right*) KcsA reconstituted in POPC/POPG (3:1, moles/moles) liposomes. Measurements at pH 7.5 and pH 4 correspond to closed and open states of the channel (*Top*). The difference in predominant peak distances (Δ Distance) is shown (*Middle*), and the difference values were mapped on the crystal structure of KcsA (1K4C) to highlight the conformational changes between different functional states of KcsA (*Bottom*) upon gating. Details are provided in *SI Materials and Methods*.

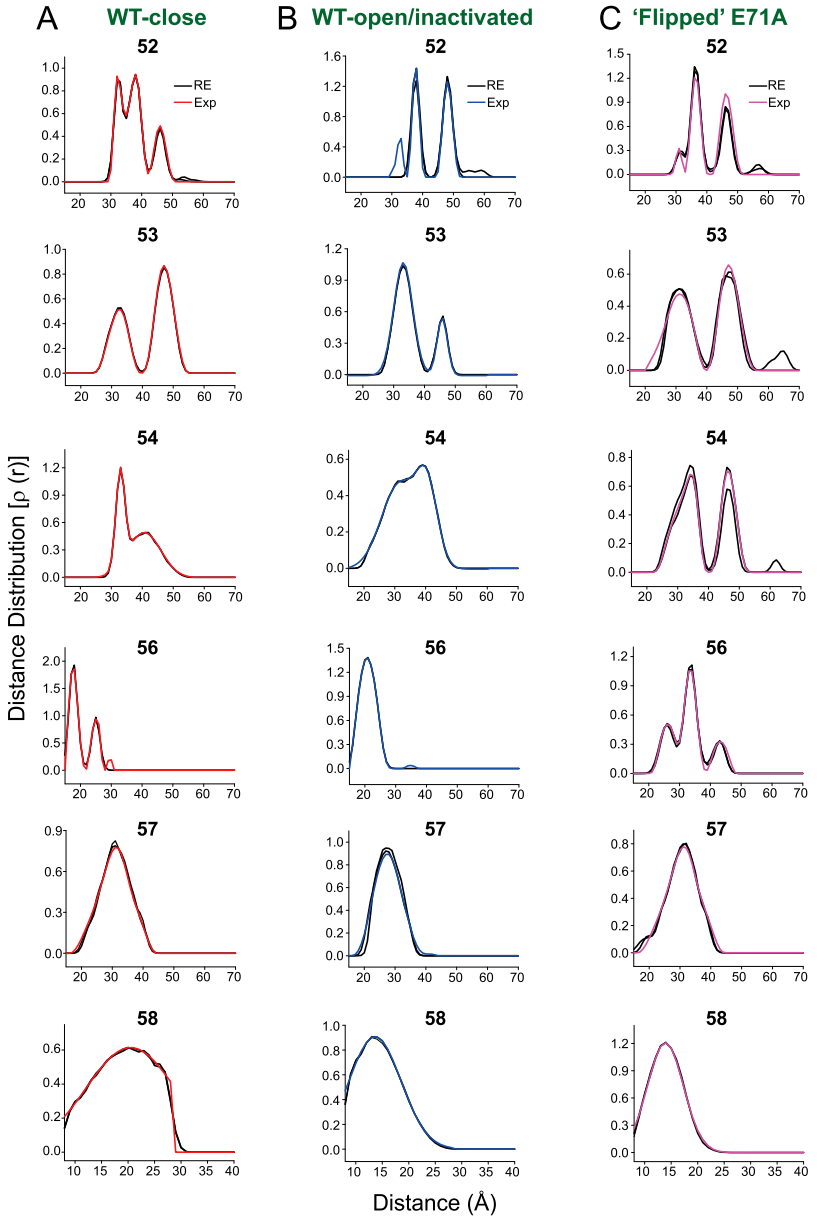

Fig. S7. Experimentally derived distance histograms and RE simulations in different functional states of KcsA. Twenty-five copies of the spin label were attached in silico to outer vestibule residues in four subunits of KcsA. The resulting 625 distances (25 * 25) between diagonally symmetrical subunits were then used to match the experimentally derived distance distributions for (*A*) WT/closed (red), (*B*) WT/open (blue), and (*C*) flipped E71A (magenta) KcsA for residues 52, 53, 54, 56, 57, and 58. The two black traces correspond to distance histograms from RE simulations from two pairs of diagonal subunits. Details are provided in *SI Materials and Methods*.

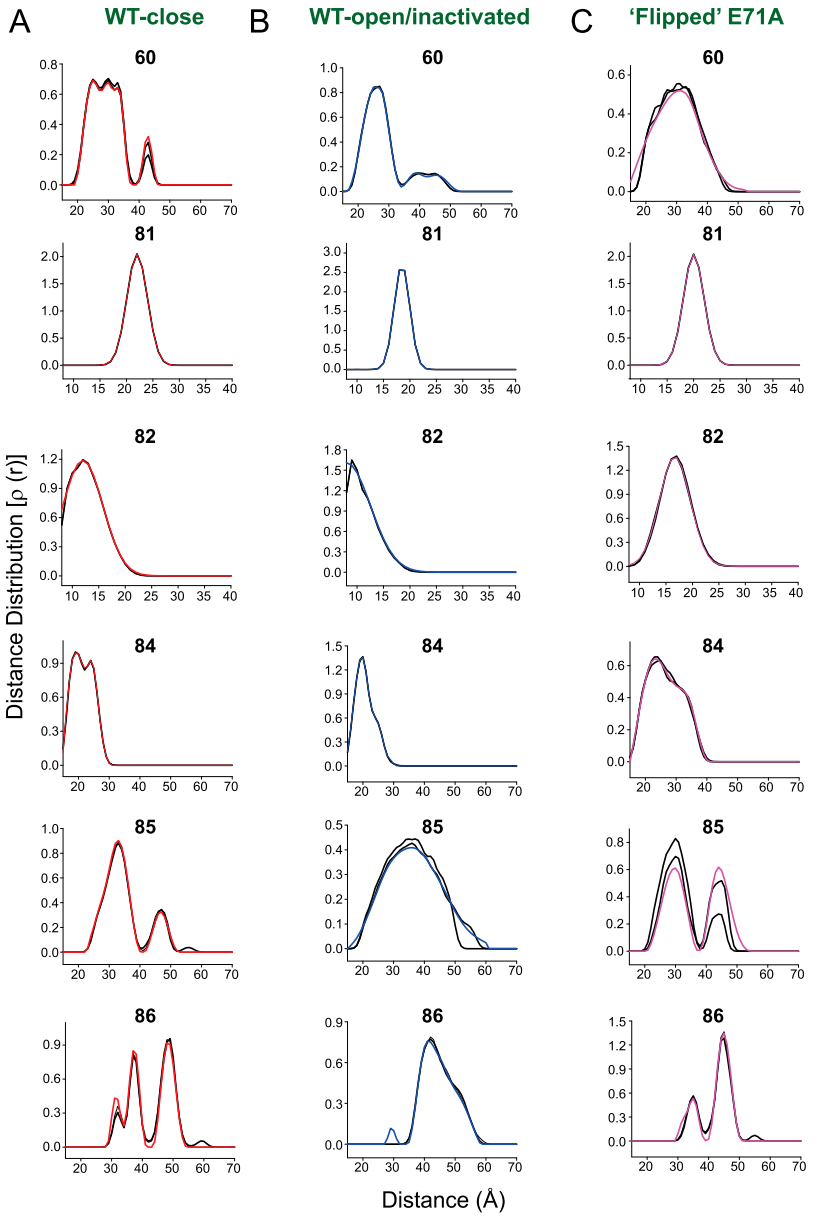

Fig. S8. Experimentally derived distance histograms and RE simulations in different functional states of KcsA. Twenty-five copies of the spin label were attached in silico to outer vestibule residues in four subunits of KcsA. The resulting 625 distances (25 * 25) between diagonally symmetrical subunits were then used to match the experimentally derived distance distributions for (*A*) WT/closed (red), (*B*) WT/open (blue), and (*C*) flipped E71A (magenta) KcsA for residues 60, 81, 82, 84, 85, and 86. The two black traces correspond to distance histograms from RE simulations from two pairs of diagonal subunits. Details are provided in *SI Materials and Methods*.

Table S1. Cα-Cα distances for outer vestibule residues between diagonally symmetrical subunits obtained from RE simulations

Residue	Closed/conductive (PDB ID code 1K4C)	Open/inactivated (PDB ID code 3F5W)	Flipped E71A (PDB ID code 2ATK)
52	44.1 (43.1)*	44.6 (43.3)	46.3 (44.3)
53	46.7 (45.9)	47.0 (45.8)	48.2 (47.0)
54	41.7 (39.7)	41.7 (39.6)	43.1 (40.9)
56	30.3 (28.8)	31.2 (29.1)	31.7 (30.0)
57	30.6 (29.8)	30.8 (30.1)	30.9 (31.2)
58	27.8 (27.4)	28.4 (27.7)	27.7 (28.2)
60	37.9 (37.2)	38.7 (37.7)	38.3 (38.0)
81	18.2 (18.4)	17.6 (18.2)	16.6 (17.2)
82	19.8 (20.2)	19.6 (20.4)	20.3 (20.7)
84	29.8 (29.2)	29.7 (29.8)	30.4 (30.9)
85	37.1 (36.5)	37.1 (37.1)	37.6 (38.0)
86	40.4 (39.9)	40.7 (40.1)	40.8 (40.7)

Distance distributions obtained by EPR using the membrane-reconstituted TD constructs of the indicated outer vestibule residues were used.

*Values in parentheses correspond to the Cα-Cα distances between diagonally symmetrical subunits from the crystal structures. Details are provided in *SI Materials and Methods* and Fig. 4.